Medial models incorporating object variability for 3D shape analysis

Martin Styner and Guido Gerig

Dept. of Computer Science, Univ. of North Carolina, Chapel Hill NC 27599, USA,
martin_styner@ieee.org, gerig@cs.unc.edu,
WWW home page: http://www.cs.unc.edu/~styner

Abstract. Knowledge about the biological variability of anatomical objects is essential for statistical shape analysis and discrimination between healthy and pathological structures. This paper describes a novel approach that incorporates variability of an object population into the generation of a characteristic 3D shape model. The proposed shape representation is based on a fine-scale spherical harmonics (SPHARM) boundary description and a coarse-scale sampled medial description. The medial description is composed of a net of medial samples (m-rep) with fixed graph properties. The medial model is computed automatically from a predefined shape space using pruned 3D Voronoi skeletons to determine the stable medial branching topology. An intrinsic coordinate system and an implicit correspondence between shapes is defined on the medial manifold. Our novel representation describes shape and shape changes in a natural and intuitive fashion. Several experimental studies of biological structures regarding shape asymmetry and similarity clearly demonstrate the meaningful represesentation of local and global form.

1 Introduction

Shape is one of the most characteristic features of objects in the real world. While humans have no apparent difficulty dealing with shapes, research in computer vision faced the usual problem when imitating human perception: humans *can* do it, but nobody knows exactly *how*. Representation and especially analysis of shape proved to be a rather complex and challenging problem. It has been shown that a generally applicable solution is not possible and that specific shape descriptions have to be established. In this paper, we present a novel framework for building shape models to be used for shape analysis.

Davatzikos et al [8] proposed an analysis of shape morphometry via a spatially normalizing elastic transformation. Inter-subject comparisons were made by comparing the individual transformations. The method is applied in 2D to a population of corpora callosa. A similar approach in 3D has been chosen by Joshi et al [11] to compare hippocampi. Using the viscous fluid transformation proposed by Miller [6], inter-subject comparisons were made by analyzing the
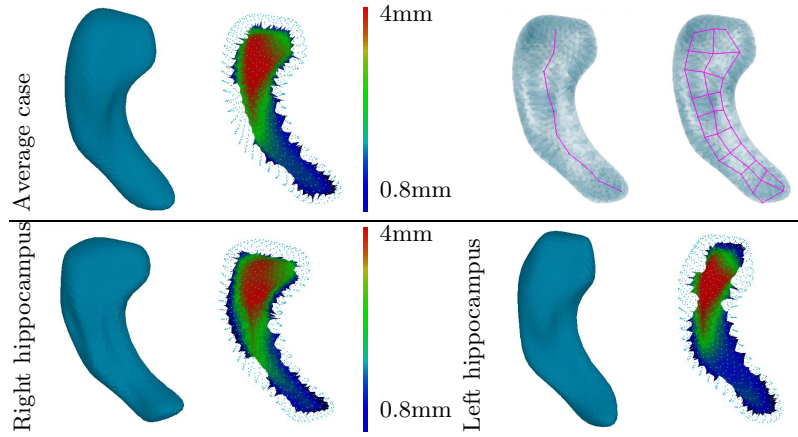
Fig. 1. Visualization of a left/right hippocampus pair with its average structure. Boundary (left), pruned Voronoi skeleton (right) with thickness coloring (same range for all objects). For the average case the medial axis and grid is shown on the top row.

transformation fields. The *analysis* of transformation fields in both methods has to cope with the high dimensionality of the transformation and the sensitivity to the initial position. Although the number of subjects in the studied populations is low, both show a relatively stable extraction of shape changes (see Csernansky [7]). The shape changes provided by the deformation fields are hard to interpret and cannot be expressed intuitively.

The INRIA group developed a feature based concept based on crest lines to represent shape variability and to built statistical atlases (Subsol [20]). The approach results in a point to point correspondence and uses a space spline transformation to warp 3D image data.

The approach taken by Kelemen [13] evaluates a population of 3D hippocampal shapes based on a boundary description by spherical harmonic basis functions (SPHARM), which was proposed by Brechbühler [3]. The SPHARM shape description delivers an implicit correspondence between shapes on the boundary, which is used in the statistical analysis. As in the approaches discussed before, this approach has to handle the problem of high dimensional features versus a low number of subjects. Further, the detected shape changes are expressed as changes of coefficients that are hard to intrepete.

Golland [10] in 2D and Pizer et al [16] in 3D proposed two different approaches of applying shape analysis to a medial shape description. Blum [4] claims that medial descriptions are based on the idea of a biological growth model and a 'natural geometry for biological shape.' The medial axis in 2D captures shape intuitively and can be related to human vision (see Burbeck [5] and Siddiqui [17]). Both Pizer and Golland propose a sampled medial model that is fitted to individual shapes. By holding the topology of the model fixed, an
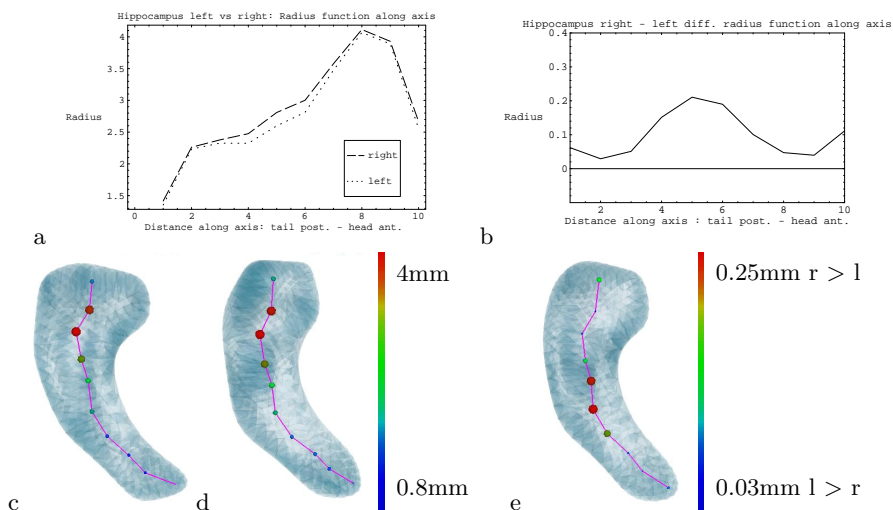
Fig. 2. Thickness asymmetry along medial axis (tail to head): a: Radius plot. b: Difference Plot: $\boldsymbol{r}_{right} - \boldsymbol{r}_{left}$. c,d: m-rep description (c: left, d: right). e: Difference $(R - L)$ at medial atoms with proportional radius/color: $r \sim |R - L|; col \sim (R - L)$.

implicit correspondence between shapes is given. So far, there was no effort to automatically construct the medial model but it has been constructed manually.

Kimia and Giblin [9] have proposed a medial hypergraph in 3D. They showed that the hypergraph completely characterizes the shape of an object. Similar to work in 2D by Siddiqi et al [18], this hypergraph could be used for shape recognition and shape design. To our knowledge, no studies have been done towards using the medial graph/hypergraph directly for shape analysis.

In this paper we present a new approach to shape analysis using both boundary and medial description. The medial description is computed automatically from a shape space of a population. The topology of the medial description is calculated by studying the topological changes of pruned 3D Voronoi skeletons. Voronoi skeletons as a shape representations have been studied intensively in past. The most influential pruning related studies regarding have been performed by Ogniewicz [15] in 2D, Naef [14] and Attali [1] in 3D.

This paper is organized as follows. In the next section, the motivation of our work is discussed guided by an example. Then, we show how a stable sampled medial description is automatically constructed in the presence of shape variability. We start with a general description and discuss shape space, common medial branching topology and minimal sampling in detail. In the result section, neuroimaging applications of shape analysis are presented.
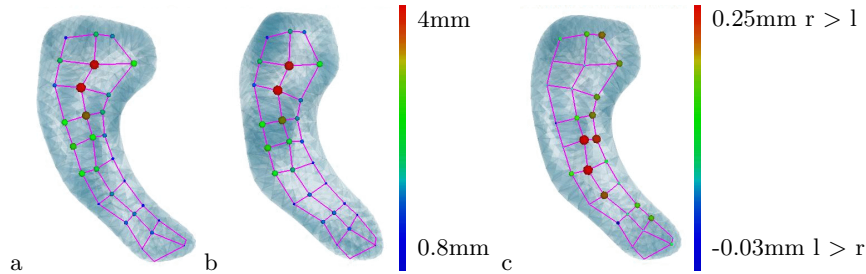
Fig. 3. Thickness asymmetry for a left/right hippocampus pair: a,b: M-rep descriptions (a: right, b: left). Radius/color are proportional to the corresponding radius. c: Difference $(R-L)$ at medial atoms with proportional radius/color: $r \sim |R-L|$; $col \sim (R-L)$.

2   Motivation: Shape analysis in an asymmetry study

This section describes an example for the intuitive description of shape changes that is inherent to the medial description. We will show an analysis of left/right asymmetry in hippocampi, a subcortical human brain structure. Asymmetry is defined via the interhemispheric plane, therefore the right hippocampus was mirrored for comparison. The main advantage of medial descriptions is the separation of the local shape properties *thickness* and *location*. In the presented case we chose to investigate mainly the thickness information of the medial manifold.

In Fig. 1 the hippocampi are visualized and asymmetry is clearly visible. Volume and medial axis length measurements indicate the same result that the right hippocampus is larger than the left: $vol_{right} = 2184mm^3$, $vol_{left} = 2023mm^3$; $axis_{right} = 65.7mm$, $axis_{left} = 64.5mm$. But these measurements do not provide a localization of the detected asymmetry. This asymmetry can easily be computed and intuitively visualized using our new medial description.

When analyzing the thickness of the hippocampi along the medial axis (the intrinsic coordinate system), we get a more localized understanding of the asymmetry. In Fig. 2 the right hippocampus is thicker over the full length of the axis, and the difference is most pronounced in the middle part of the axis. In order to relate this thickness information with the appropriate location, we visualize it in the medial samples itself. Each medial atom (sample of the medial surface) is displayed by a sphere of size and color that is proportional to its thickness. This kind of display can also be used to visualize the thickness difference of corresponding locations in the right and left hippocampus. The sphere radius and color is proportional to the difference: $r \sim |R - L|$; $col \sim (R - L)$ (see Fig. 2).

As a next step, we take into account a grid of medial atoms and perform the same analysis as for the axis (see Fig. 3). We observe that the right shape is thicker, but the difference is most pronounced in the middle part.

All parts of the processing are described in the methods section and more detailed examples are presented in the results section. The applied methods computed the medial branching topology of one single sheet with volumetric
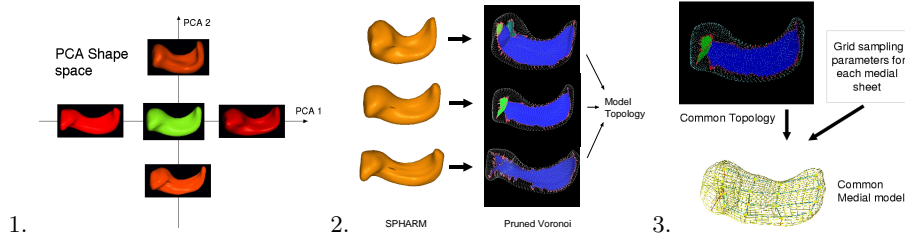
Fig. 4. Computation of a medial model from an object population. 1. Shape space definition. 2. Common medial branching extraction. 3. Compute minimal sampling.

overlap larger than 98% and approximation error less than 10% MAD_{norm} (Mean Absolute Distance).

It is evident that in the presented hippocampus study the medial description gives a better understanding of the observed asymmetry than simple measurements like volume or even the length of the medial axis. Limiting ourself to a coarse scale description does not lessen the power of the analysis and asymmetry can reliably be detected and localized. In the result section, we present another example dealing with asymmetry in a lateral ventricles study.

3   Methods

The main problem for a medial shape analysis is the determination of a stable medial model in the presence of biological shape variability. Given a population of anatomical objects, how can we determine a stable medial model automatically? This section describes the methods that were developed to construct such an medial model. Some parts were described in more detail by Styner [19].

Our scheme is subdivided into 3 steps and visualized in Fig. 4. We first define a shape space for our computations using Principal Component Analysis. From this shape space, we generate the medial model in two distinct steps. First, we compute the common branching topology using pruned Voronoi skeletons. Secondly, we calculate the minimal sampling of the medial manifold given a predefined maximal approximation error in the shape space.

3.1   SPHARM and m-rep shape description

Two shape description are of importance in this work: a) the boundary description using SPHARM and b) the medial description using m-rep.

The SPHARM description (see Brechbühler [3]) is a global, fine scale description that representa shapes of sphere topology. The basis functions of the parameterized surface are spherical harmonics, which have been demonstrated by Kelemen [13] to be non-critical to shape deformations. SPHARM is a smooth, accurate surface shape representation given a sufficiently small approximation

error. Based on a uniform icosahedron-subdivision of the spherical parameterization, we obtain a Point Distribution Model (PDM) directly from the coefficients via a linear mapping $x = A \cdot c$. Correspondence of SPHARM is determined by normalizing the parameterization to the first order ellipsoid.

M-rep is a local medial shape description. It is a set of linked samples, called medial atoms, $m = (\boldsymbol{x}, r, \underline{F}, \theta)$ (see Pizer et al [16]). Each atom is composed of: 1) a position $\boldsymbol{x}$, 2) a width r, 3) a frame $\underline{F}$ implying the tangent plane to the medial manifold and 4) an object angle θ. A figure is a non-branching medial sheet. Figures are connected via inter-figural links. The medial atoms form a graph with edges representing either inter- or intra-figural links. In the generic case, this medial graph is non-planar, i.e. overlapping when displayed in a 2D diagram. The sampling is sparse and leads to a coarse scale description. Correspondence between shapes is implicitly given if the medial graphs are equivalent. We express every shape by the same medial graph varying only the parameters of the medial atoms. For every population of similar shapes there is a specific medial graph.

3.2   Shape space

We define a shape space via the population average and its major deformation modes (eigenmodes) determined by a principal component analysis (PCA). We compute the SPHARM shape representations $\boldsymbol{c}_i$ for a population and apply PCA to the coefficients as described by Kelemen [13]. The eigenmodes $(\lambda_i, \boldsymbol{p}_i)$ in the shape space cover at least 95% of the variability in the population:

$$\Sigma = \frac{1}{n-1} \sum_i (\boldsymbol{c}_i - \bar{\boldsymbol{c}}) \cdot (\boldsymbol{c}_i - \bar{\boldsymbol{c}})^T \tag{1}$$

$$0 = (\Sigma - \lambda_i \cdot I_n) \cdot \boldsymbol{p}_i; i = 1 \ldots n-1 \tag{2}$$

$$Space_{\text{shape}} = \{\bar{\boldsymbol{c}} \pm 2 \cdot \sqrt{\lambda_i} \cdot \boldsymbol{p}_i\}; i = 1 \ldots k_{95\%} \tag{3}$$

Since the shape space is continuous, we need to determine a shape set by a representative sampling of the shape space. All computations are then applied to the shape set. The number of shapes in this set can be considerably higher than the original number of shapes (see section 4.1 for an example).

3.3   Computing a common medial branching topology

In this section, we describe how the common medial branching topology is computed in a three step approach. First, we compute for each member of the shape set its branching topology. Then we establish a common spatial frame in order to compare the topology of different shapes. As a last step we determine the common topology via a spatial matching criterion in the common frame.

Branching topology of a single shape - The branching topology for a single shape is derived via Voronoi skeletons (see Attali [1]). In order to calculate the 3D Voronoi skeleton from the SPHARM description, we first calculate a finely sampled PDM. From the PDM, the inside 3D Voronoi diagram is calculated. The
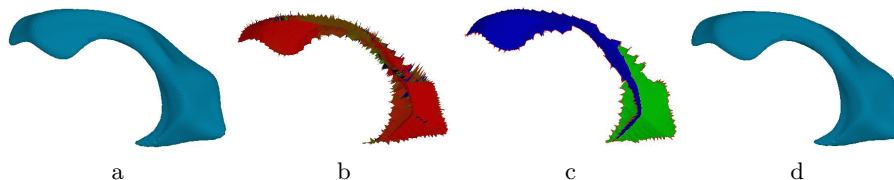
Fig. 5. Voronoi skeleton pruning scheme applied to a lateral ventricles (side views). a. Original ventricle. b: Original Voronoi skeleton (~ 1600 sheets). d: Pruned skeleton (2 sheets). c: Reconstruction from pruned skeleton ($E_{\mathrm{overlap}} = 98.3\%$).

Voronoi diagram is well behaved due to the fact that the PDM is a fine sampling of the smooth SPHARM. The medial manifold of a Voronoi skeleton is described by Voronoi vertices connected by Voronoi edges forming planar Voronoi faces. A face-grouping algorithm was developed that is based on the grouping algorithm proposed by Naef [14]. The algorithm groups the Voronoi faces into a set of medial sheets. It is a graph algorithm that uses a cost function weighted by a geometric continuity criterion. Additionally a merging step has been implemented, which merges similar sheets according to a mixed radial and geometric continuity criterion. The computed medial sheets are weighted by their volumetric contribution to the overall object volume: $C_{sheet} = (vol_{skel} - vol_{skel \setminus sheet_i})/vol_{skel}$. The medial sheet are then pruned using a topology preserving deletion scheme. An example of the scheme is presented in Fig. 5. We are aware that this pruning scheme has to be adapted when dealing with very complex objects like the whole brain cortex.

A common spatial frame for branching topology comparison - The problem of comparing branching topologies has already been adressed before in 2D by Siddiqi [18] and others, mainly via matching medial graphs. So far, there is little work done in 3D. The results in 2D and August [2] have shown that the medial branching topology is quite unstable. In 3D, the medial branching topology is even more unstable and ambiguous as in 2D. Thus, we chose to develop a matching algorithm that does matching based on spatial correspondence. In order to apply such an algorithm, we first have to define a common spatial frame.

Our choice for a common frame is the average case of the shape space. We map each member of the shape set into the common frame using the correspondence that is given on the boundary. The SPHARM description defines a boundary correspondence via the first order ellipsoid. This correspondence is carried through to the derived PDM, which is the basis of the branching topology computation. By mapping every PDM into the PDM of the common frame, we perfectly overlap the sampled boundaries of every object. To map the whole 3D space, we use a Thin-Plate-Spline warp algorithm. Thus, we warp every skeleton into the common frame, where all their boundaries match perfectly.

Extraction of a common topology - Given that all objects were mapped into a common spatial frame, we can define a matching criterion between the
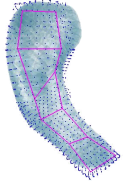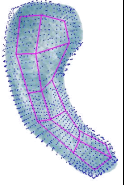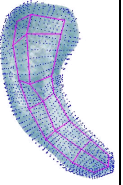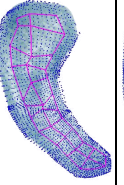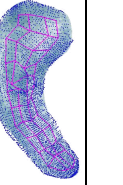
m-rep					
Grid	2x6	3x6	3x7	3x12	4x12
$I.\mathrm{MAD}_{norm}$	0.159	0.116	0.109	0.066	0.051
$II.\mathrm{MAD}_{norm}$	0.146	0.076	0.075	0.053	0.048

Fig. 6. Sampling approximation errors of the implied surface from a hippocampus structure in the initial position (I) and after deformation (II). The Mean Absolute Distance (MAD) is normalized with the average radius: $r_{avg} = 2.67$ mm. The images show the m-rep (red lines), points of the implied boundary (dark blue dots) and the original boundary (light blue transparent).

medial sheets. We visually observed a very high degree of overlap between matching sheets in the common frame. Thus, we chose to use the spatial distribution of the Voronoi vertices of every sheet. The matching criterion is defined as the paired Mahanolobis distance. It is a non-Euclidean distance measure that takes into account the non-isotropic distribution of the vertices. We determined an empirical threshold that represents the rejection of a match if the centers of the spatial distributions are further away than 2 standard deviations.

$$f_{dist}(\{\mu_1, \Sigma_1\}, \{\mu_2, \Sigma_2\}) = (M(\mu_1, \Sigma_1, \mu_2) + M(\mu_2, \Sigma_2, \mu_1))/2 \qquad (4)$$

$$M(\mu, \Sigma, \boldsymbol{x}) = \parallel \Sigma^{-1} \cdot (\mu - \boldsymbol{x}) \parallel_2 \qquad (5)$$

The matching procedure starts by assigning the topology of the average case as the initial common topology. The common topology is step by step refined by comparing it to every member in the shape set. All medial sheets that were judged to be non-matching are incorporated into the common topology. This matching procedure does a one-to-many match, since due to skeletal instabilities a single medial sheet in one shape can have two or more corresponding sheets in another shape. The resulting common topology is a set of medial sheets originating from members of the shape set.

3.4   Computing the minimal sampling of the medial manifold

From the common branching topology we compute the sampling of the associated sheets by a grid of medial atoms. The m-rep model is determined by the common branching topology and a set of parameters that specify the grid dimensions for each sheet. The sampling algorithm is based on the longest 1D thinning axis of the edge-smoothed 3D medial sheet. A detailed description of the algorithm would exceed the scope of this paper and thus is omitted here.
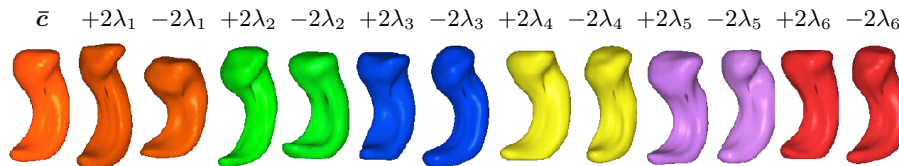
$$\bar{c} \quad +2\lambda_1 \quad -2\lambda_1 \quad +2\lambda_2 \quad -2\lambda_2 \quad +2\lambda_3 \quad -2\lambda_3 \quad +2\lambda_4 \quad -2\lambda_4 \quad +2\lambda_5 \quad -2\lambda_5 \quad +2\lambda_6 \quad -2\lambda_6$$

Fig. 7. Subset of the shapeset from a PCA shape space for a pooled Control-Schizophrenia population: Average case with deformations along eigenmodes.

The set of grid parameters is optimized to be minimal while the corresponding m-rep deforms into every member of the shape set with a predefined maximal approximation error. The approximation error is computed as Mean Absolute Distance (MAD) of the implied and the original boundary. In order to have an error independent of the object size, we normalize with the average radius of the skeleton: $\mathrm{MAD}_{norm} = \mathrm{MAD}/r_{avg}$. In Fig. 6 we show the error of various sampling parameters. The limiting error was chosen at 10% of the average radius.

3.5 Deforming the m-rep into an individual shape

Once a m-rep model is computed, we want to fit it into individual shapes. This fit is done in two steps. First we obtain a good initial estimate which is then refined in a second step to fit to the boundary. The initial estimate is obtained by warping the m-rep model from the common frame into the frame of the individual shape using the correspondence on the boundary given by the PDM.

From that position we run an optimization that changes the features of the m-rep atoms to improve the fit to the boundary (see Joshi [12]). Local similarity transformations as well as rotations of the local angulation are applied to the medial atoms. The fit to the boundary is constrained by an additional Markov random field prior that guarantees the smoothness of the medial manifold.

3.6 Issues of Stability

We consider the stability of the common medial branching topology to be good. Several experiments with various anatomical objects confirmed this hypothesis. The least stable part of the common topology is its dependency on the boundary correspondence for the topology matching procedure. Although we did not yet experience problems with the quality of the boundary correspondence, it is evident that for objects with a high degree of rotational symmetry our first order ellipsoid correspondence is not appropriate. The borders of the Voronoi skeleton are sensitive to small perturbations on the boundary, unlike the center part of the skeleton which is quite stable. Thus, the sampled medial grid is quite stable in its center, but rather unstable at the edges. The parameters of the grid sampling (rows, columns) are neither very stable, nor unstable.
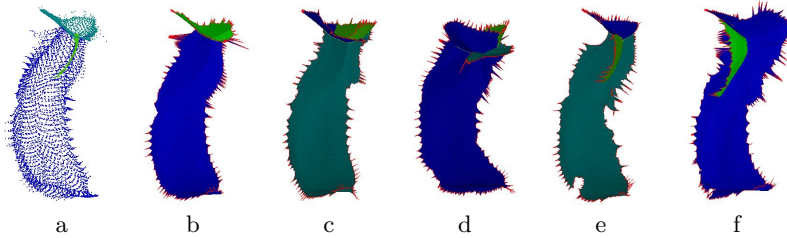
Fig. 8. Topology matching scheme applied to the shape space of hippocampus-amygdala objects. a: Final topology with 3 medial sheets as clouds of Voronoi Vertices. b-f: Examples of members from the shape set.

If we compute the common medial model for 2 similar populations (e.g. 2 different studies of the same object regarding the same disease), we expect the same medial branching topology, similar grid parameters, and very similar m-rep properties in the center, but unlikely similar m-rep properties at the boundaries of the grid. We are currently verifying this hypothesis. Because we construct the model only once and its extraction is deterministic and repeatable, the stability of a medial model for a single population is regarded as stable.

4   Results

4.1   Medial model for a hippocampus-amygdala population

The main contribution in this paper is the scheme to extract a medial model that incorporates biological variability. This section presents the scheme applied to a hippocampus-amygdala population from a schizophrenia study (30 subjects).

The SPHARM coefficients were determined and normalized regarding rotation and translation using the first order ellipsoid. The scale was normalized with the individual volume. The first 6 eigenmodes λ_i of the PCA shape space contain 97% of the variability in the population and thus the shape space is defined as $\{\bar{c} \pm 2 \cdot \sqrt{\lambda_i}; i = 1 \ldots 6\}$. The shape set was computed by uniformly sampling 5 shapes along each eigenmode (see Fig. 7 for a subset).

The 3D Voronoi skeletons were computed from the PDM's and pruned. No member of the shape set had a branching topology comprised by more than 4 medial sheets. In Fig. 8 the individual medial topology of several members of the shape set are displayed together with the common medial topology, which consists of only three medial sheets. Every member of the shape set had a volumetric overlap larger than 98% of the reconstruction with the original object. The minimal sampling of the medial topology was computed with an maximal $\mathrm{MAD}_{norm} \leq 0.1$. The application of the m-rep model to all individual cases did not produce a MAD_{norm} larger than 0.1 (see also Fig. 9). This highly encouraging result strengthens the validity of our assumptions in the proposed scheme.

	Boundary	Skeleton	$E_{overlap}$	Init. m-rep	E_{MAD}	Def. m-rep	E_{MAD}
$\bar{c}$			98.64%		0.081		0.069
$\bar{c}$ $+$ $2 \cdot \lambda_2$			98.35%		0.118		0.099
Case			98.02%		0.185		0.096

Fig. 9. Approximation errors: The common model applied to the average (top), a shape set member (middle) and an individual case (bottom). The pruned Voronoi skeletons and the volumetric overlap is presented. In the middle columns, the initial m-rep (after the warp) and its MAD_{norm} error is displayed ($r_{avg} = 3.6mm$). On the right, one can see the deformed m-rep and the corresponding MAD_{norm}. After deformation, the lower boundary for the MAD_{norm} error (≤ 0.10) was satisfied for all shapes.

4.2   Asymmetry analysis of lateral ventricles of twins

This section presents our scheme applied to a population of lateral ventricles, a fluid filled structure in the center of the human brain. The data is from a Mono/Di-zygotic twin study and consists of 20 twin subjects (10 pairs, 5 each).

In order to do asymmetry analysis, we mirrored the left objects at the interhemispheric plane. The SPHARM coefficients were determined and normalized regarding rotation and translation using the first order ellipsoid. The scale was normalized by the individual volume. In Fig. 11 the SPHARM correspondence is shown. The first 8 eigenmodes λ_i of the PCA shape space contain 96% of the variability in the population and thus the shape space is defined as $\{\bar{c} \pm 2 \cdot \sqrt{\lambda_i}; i = 1 \ldots 8\}$. The PDM of the shape set was computed and a common medial branching topology for all objects using Voronoi skeletons was determined. The medial branching topology consisted of one to three medial sheets with an volumetric overlap of more than 98% for each. The common medial topology was computed to be a single sheet.

The minimal sampling of the medial topology was computed with an maximal $\mathrm{MAD}_{norm} \leq 0.1$ in the shape space. The application of the medial model to all individual cases did not produce a MAD_{norm} larger than 0.1, which is
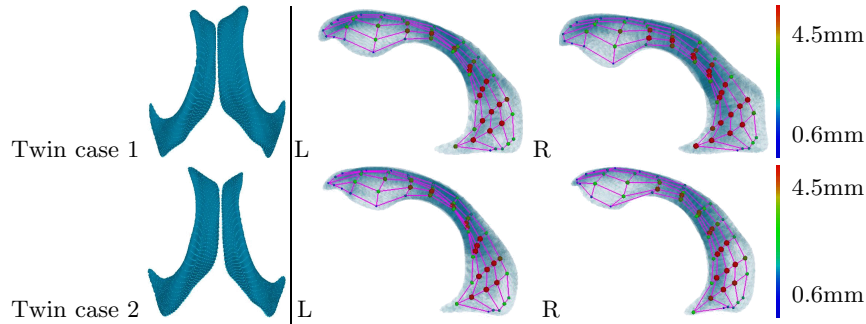
Fig. 10. Visualization of the lateral ventricles of two monozygotic twins and its corresponding m-reps. Radius/color is proportional to the thickness. The figure shows a clear asymmetry in both cases of the boundary display.

about 0.35mm. Since the lateral ventricle is a thin, long structure (medial axis $\sim$ 115mm), this is a very small error for a coarse scale description.

We examined a monozygotic twin pair more closely for an asymmetry and similarity analysis (see Fig. 10). An asymmetry is clearly present, also in the volume measurements: twin 1 $L/R = 9365/12442mm^3$; twin 2 $L/R = 8724/6929mm^3$. An analysis of the thickness is shown in Fig. 12. It is obvious, that the asymmetry in the twin 1 is considerably higher than in twin 2. Moreover, the similarity is much higher on the left side than on the right.

5   Conclusions and Discussion

We present a new approach to the description and analysis of shape for objects in the presence of biological variability. The proposed description is based on a boundary and a medial description. Using the medial description we can visualize and quantitate locally computed shape features regarding asymmetry or similarity. Since a correspondence is given on both the boundary and the medial manifold a statistical analysis can be directly applied. We showed several shape analysis examples of the medial description and the results are very encouraging.

The choice of a *fixed* topology for the m-rep has several advantages, e.g. enabling an implicit correspondence for statistical analysis. On the other hand, a fixed topology m-rep model cannot precisely capture the topology of an individual object. The determined m-rep is therefore always an approximation, which emphasizes our decision of a coarse scale m-rep description.

The SPHARM description and thus also the derived m-rep is constrained to objects of sphere topology. The SPHARM boundary correspondence has shown to be a good approach in the general case, but it has inherent problems e.g. in case of rotational symmetry.

This paper describes a scheme which is work in progress. All parts of the scheme have already been implemented, applied and tested. The scheme has been
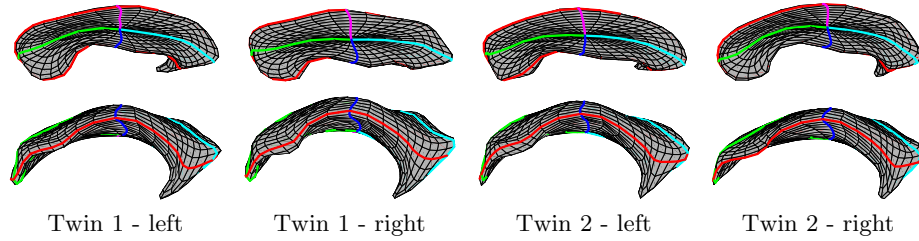
Twin 1 - left   Twin 1 - right   Twin 2 - left   Twin 2 - right

Fig. 11. Visualization of the normalization SPHARM parameterization net using the first order ellipsoid for the lateral ventricle example. The top row shows a top view and the bottom row a side view. The three axes are in corresponding colors.
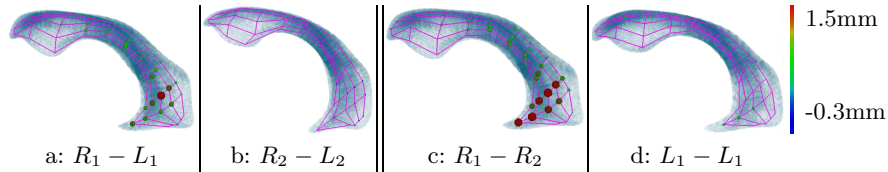

a: $R_1 - L_1$ b: $R_2 - L_2$ c: $R_1 - R_2$ d: $L_1 - L_1$

Fig. 12. Asymmetry/similarity analysis of the thickness. M-rep radius and color is proportional to the difference (the same range has been applied to all objects). Maximal differences: a) 1.5mm, b) 0.28mm, c) 1.7mm, d) 0.42mm. In the first twin there is a higher degree of asymmetry. The similarity of the left side is higher than the right side.

applied to populations of several structures of neurological interest: amygdala-hippocampus(60 cases), hippocampus(20), thalamus(56), globus pallidus(56), putamen(56) and lateral ventricles(40). The generation of the medial description takes into account the biological variability of a set of training shapes, which is a novel concept. We have shown that we can compute a stable medial description for a population of shapes. The biological variability is captured efficiently, and therefore it is a step further towards a natural shape representation.

As next steps, we have to study the robustness of our scheme and to apply shape statistics for discrimination and similarity studies. Methods for statistical shape analysis of medial structures have been performed at our lab in 2D (Yushkevich [21]). Applications to clinical studies in Schizophrenia and other neurological diseases are in progress.

Acknowledgments

References

1. Attali, D. and Sanniti di Baja, G. and E. Thiel: Skeleton simplification through non significant branch removal. Image Proc. and Comm. (1997) **3** 63–72
2. August, J. and Siddiqi, K. and Zucker, S.: Ligature instabilities in the perceptual organization of shape. Computer Vision and Pattern Recognition (1999)
3. Brechbühler, C.: Description and analysis of 3-D shapes by Parametrization of closed surfaces. (1995), Dissertation, IKT/BIWI, ETH Zürich, Hartung Gorre
4. Blum, T.O: A transformation for extracting new descriptors of shape. Models for the Perception of Speech and Visual Form (1967) MIT Press
5. Burbeck, C.A. and Pizer, S.M and Morse, B.S. and Ariely, D. and Zauberman, G. and Rolland, J.: Linking object boundaries at scale: a common mechanism for size and shape judgments. Vision Research (1996) **36** 361–372,
6. Christensen, G.E. and Rabbitt, R.D. and Miller, M.I.: 3D brain mapping using a deformable neuroanatomy. Physics in Medicine and Biology (1994) **39** 209–618
7. Csernansky, JG and Joshi, S and Haller, J and Gado, M and Miller, JP and Grenander, U and Miller, MI: Hippocampal morphometry in Schizophrenia via high dimensional brain mapping. Proc. Natl. Acad. Sci. USA (1998) **95** 11406–11411
8. Davatzikos, D. and Vaillant, M. and Resnick, S. and Prince, J.L and Letovsky, S. and Bryan, R.N.: A computerized method for morphological analysis of the Corpus Callosum. Comp. Ass. Tomography (1998) **20** 88–97
9. Giblin, P. and Kimia, B.: A formal classification of 3D medial axis points and their local geometry. Computer Vision and Pattern Recognition (2000) 566–573
10. Golland, P. and Grimson, W.E.L. and Kikinis, R.: Statistical shape analysis using fixed topology skeletons: Corpus Callosum study. IPMI (1999) LNCS 1613,382–388
11. Joshi, S. and Miller, M and Grenander, U.: On the geometry and shape of brain sub-manifolds. Pat. Rec. and Art. Intel. (1997) **11**, 1317–1343
12. Joshi, S. and Pizer, S. and Fletcher, T. and Thall, A. and Tracton, G.: Multi-scale deformable model segmentation based on medial description. IPMI (2001)
13. Kelemen, András and Székely, Gábor and Gerig, Guido: Elastic model-based segmentation of 3D neuroradiological datasets. IEEE Med. Imaging (1999) **18** 828–839
14. Näf, M.: Voronoi skeletons: a semicontinous implementation of the 'Symmetric Axis Transform' in 3D space. ETH Zürich, IKT/BIWI (1996), Dissertation
15. Ogniewicz, R. and Ilg, M.: Voronoi skeletons: theory and applications. Computer Vision and Pattern Recognition (1992) 63–69
16. Pizer, S. and Fritsch, D. and Yushkevich, P. and Johnson, V. and Chaney, E.: Segmentation, registration, and measurement of shape variation via image object Shape. IEEE Transactions on Medical Imaging (1999) **18** 851–865
17. Siddiqi, K. and Kimia, B. and Zucker, S. and Tannenbaum, A.: Shape, shocks and wiggles. Image and Vision Computing Journal (1999) **17** 365–373

18. Siddiqi, K. and Ahokoufandeh, A. and Dickinson, S. and Zucker, S.: Shock graphs and shape matching. Computer Vision (1999) **35** 13–32

19. Styner, M and Gerig, G.: Hybrid boundary-medial shape description for biologically variable shapes. Math. Methods in Biomedical Image Analysis (2000) 235–242

20. Subsol, G and Thirion, J.P. and Ayache, N.: A scheme for automatically building three-dimensional morphometric anatomical atlases: application to a skull atlas. Medical Image Analysis (1998), **2** 37–60

21. Yushkevich, P. and Pizer, S.: Coarse to fine shape analysis via medial models. IPMI (2001)